Computational Study of Acidic and Basic Functionalized Crystalline Silica Surfaces as a Model for Biomaterial Interfaces

Corno, Marta; Delle Piane, Massimo; Monti, Susanna; Moreno-Couranjou, Maryline; Choquet, Patrick; Ugliengo, Piero. Computational Study of Acidic and Basic Functionalized Crystalline Silica Surfaces as a Model for Biomaterial Interfaces. LANGMUIR. 31 (23) pp: 6321-6331.
DOI: 10.1021/acs.langmuir.5b01828

A computational study of acidic and basic functionalized crystalline silica surfaces as model for biomaterial interfaces

Journal:	*Langmuir*
Manuscript ID:	la-2014-04490u
Manuscript Type:	Article
Date Submitted by the Author:	17-Nov-2014

Complete List of Authors:
Corno, Marta; Università di Torino, Dipartimento di Chimica
Delle Piane, Massimo; Università di Torino, Dipartimento di Chimica
Monti, S; CNR Institute of Chemistry of Organometallic Compounds, Area della Ricerca
Moreno-Couranjou, Maryline; Centre de Recherche Public - Gabriel Lippmann , Science and Analysis of Materials
Choquet, Patrick; CRP - Gabriel Lippmann, Département Science et Analyse des Matériaux
Ugliengo, Piero; University of Turin, Dipartimento di Chimica

A computational study of acidic and basic functionalized crystalline silica surfaces as model for biomaterial interfaces

Marta Corno[1]*, *Massimo Delle Piane*[1], *Susanna Monti*[2], *Maryline Moreno-Couranjou*[3], *Patrick Choquet*[3], *Piero Ugliengo*[1]

[1]Dipartimento di Chimica and NIS – Nanostructured Interfaces and Surfaces – Centre, Università degli Studi di Torino, via P. Giuria 7, 10125, Torino, Italy

[2]CNR Institute of Chemistry of Organometallic Compounds, Area della Ricerca, via G. Moruzzi l, I-56124 Pisa, Italy

[3]Science and Analysis of Materials Department, Centre de Recherche Public – Gabriel Lippmann, Belvaux, L-4422, Luxembourg

*Corresponding author: marta.corno@unito.it, telephone: +390116704596

Keywords. DFT methods; Reax-FF; Ab-initio; silica surfaces; functionalization; Molecular-Dynamics simulations; CRYSTAL code; biomaterial interfaces.

Abstract

In silico modeling of acidic (CH_2COOH) or basic (CH_2NH_2) functionalized silica surfaces has been carried out by means of a density functional approach based on gradient corrected functional. Hydroxylated surfaces of crystalline cristobalite (sporting 4.8 OH/nm^2) were adopted as pristine material to mimic an amorphous silica interface. The functionalization was studied by transforming the surface Si-OH groups into Si-CH_2COOH and Si-CH_2NH_2 moieties. Structures, energetics, electronic and vibrational properties were computed and compared as a function of the increasing loading of the functional groups (from 1 to 4 *per* surface unit cell). Classical molecular dynamics simulations of selected cases have been performed through Reax-FF reactive force field to assess the mobility of the surface added chains. Both DFT and force field calculations identify the CH_2NH_2 moderate surface loading (1 group *per* unit cell) as the most stable functionalization, at variance with the case of the CH_2COOH group where higher loadings are preferred (2 groups *per* unit cell). The vibrational fingerprints of the surface functionalities, which are the ν(C=O) stretching and δ(NH_2) bending modes, have been characterized for each substitution percentage in order to guide the assignment of the experimental data. The final results highlighted a different behavior of the two types of functionalization. On the one hand, the frequency associated to the ν(C=O) mode shifts to lower wavenumbers as a function of the H-bond strength between the surface functionalities (both COOH and SiOH groups); and on the other hand, the δ(NH_2) frequency shift seems caused by a subtle balance between the H-bond donor and acceptor abilities of the NH_2 moiety. Both data are in general agreement with experimental measurements on the corresponding silica functionalized materials. Present results give confidence on the future development of functionalized silica layers based on more realistic amorphous silica models.

Introduction

During the last few years the development of new effective materials for medical applications has been focused on the creation of highly biocompatible hybrid systems made of inorganic supports, such as metals, metal alloys, metal oxides, etc., and biomolecular adsorbates, such as short organic chains, amino acids, oligopeptides, etc., with specific recognition properties. Research in this field has demonstrated that the stability and efficiency of these combinations crucially depend on the physicochemical properties, dynamics and reactive phenomena, which take place at their interface. Therefore, a great number of studies has been devoted to find the most appropriate surface decoration strategies, which could impart to the final devices the desired characteristics.[1-2]

For instance, chemical modification of the material surface by covalent attach of organic moieties, namely alkyls, carboxylic and sulfonic acids, amines, alcohols, etc., implies changing the electrostatics and the hydrophilic/hydrophobic behavior of the surface.[3-4] This can be important for inducing and regulating specific events at the interface, such as a fast adsorption of selected molecules with improved electrostatic match of the complementary regions.[5]

Among the most widespread inorganic materials for biomedical applications, silicon dioxide (SiO_2, silica) has proven particularly successful, being easily manufactured, versatile and, in its amorphous form, mostly biocompatible.[5] In nanomedicine, silica is of great interest because it can be synthesized as nanoparticles for intracellular targeting and delivery.[6] Moreover, the discovery of how to prepare silica in a mesoporous form[7] (characterized by an ordered arrangement of pores of 3-30 nm in diameter) has paved the way for new and more advanced applications to drug delivery, imaging and targeting.[6,8-9] In standard conditions, silica surfaces are known to expose Si-OH (silanol) groups in a variable concentration, depending on the preparation.[10-11] These silanols are the key elements of the interaction between silica based materials and biomolecules. Additionally, silica chemistry is particularly favorable to surface functionalization with a large range of organic groups, further

expanding the applicability of this class of materials to (nano)medicine.[3,8,12-13] Generally, functionalization of silica surfaces results in the substitution of a variable number of surface silanol groups with the desired organic terminations. This process may take place through chemical modification of a previously synthesized silica material ("grafting") or during synthesis, by mixing silica and organosilica precursors ("co-condensation").[3,14-15] The former has the advantage of retaining the structure of the pure silica material, while the latter can create structural defects.[3] Among all, silica functionalization with carboxylic (-COOH) and amino ($-NH_2$) groups has been notably studied for biological applications, because these groups can form quite strong interactions with different kinds of adsorbates, therefore acting as efficient anchoring sites for the immobilization of biomolecular systems.[8] Indeed, carboxyl and amino functionalities, which have weak acid and basic characters, respectively, can be used as pH-modulators to create responsive silica surfaces, and in general bioactive materials.[8,16]

Several experimental works have focused their investigations on the effect of surface functionalization and properties and activity of silica-based materials (especially in their mesoporous form).[3] Organic functionalized groups have successfully been used to modulate the adsorption of peptides,[12] proteins[17] and DNA[18] on silica. Functionalization revealed to be fundamental in the regulation of cell uptake of mesoporous silica nanoparticles,[19] in drug delivery, where the loading of a broader range of pharmaceutical compounds was obtained, and in tuning release rates.[9,20] However, much less attention has been paid to the study of silica functionalization at a molecular level, for understanding the surface chemical structures of such engineered materials. To the best of our knowledge, only few experimental works deal with spectrophotometrical,[21] nuclear magnetic resonance[22] or X-ray diffraction[8] methods. Recently, an experimental investigation on nisin (an antimicrobial peptide) covalently grafted to a stainless steel substrate, through functionalization of the top thin layer with carboxylic groups (via atmospheric pressure dielectric barrier discharge plasma[23]) has been published. In this context,

simulations can be very useful since they can act as a "virtual microscope" to study the local environment of the surface functionalities, their interactions and their effect on experimental measurements. Nevertheless, while lot of work has concerned modeling plain silica surfaces,[24] functionalized silica substrates have been overlooked. Actually, most of the theoretical investigations rely on classical description of these systems, obtained by means of force field based molecular dynamics (MD) or grand canonical Monte Carlo (GCMC) simulations. These methods revealed to be able to disclose accurately the interactions of functionalized silica materials with molecules, such as CO_2 and N_2.[14,25-28] On the contrary, only some quantum chemistry density functional theory (DFT) calculations are present in the literature so far, and all of them deal with the modeling of small molecular clusters as representatives of the local chemical environment around the silica functionalities.[22,29]

In the present work, we report a thorough computational study, where both static DFT calculations, based on the PBE functional, and classical MD simulations, based on the reactive force field ReaxFF, are used to obtain a more complete picture of acidic and basic functionalized silica surfaces. More specifically, the substitution of surface silanols of a crystalline cristobalite model[30] with CH_2COOH and CH_2NH_2 groups is investigated and described in detail. Moreover, infrared spectra have been simulated to provide a direct comparison with experimental measurements.

Computational details

DFT calculations

For all the static calculations, we adopted the Density Functional Theory framework with the General Gradient Approximation-Perdew-Burke-Ernzerhof (DFT-GGA-PBE)[31] as encoded in the periodic CYSTAL09 code.[32-34] We chose a localized Gaussian functions basis set of polarized double-zeta quality for describing electrons as follows: 6-21G(d) for Si (α_{sp}=0.130 bohr^{-2} and α_d=0.500 bohr^{-2});[35]

6-31G(d) for O (α_{sp}=0.274 bohr^{-2} and α_d=0.538 bohr^{-2});[36] 6-21G(d) for C (α_{sp}=0.260 bohr^{-2} and α_d=0.800 bohr^{-2});[37] 6-31G(d) for N(α_{sp}=0.212 bohr^{-2} and α_d=0.800 bohr^{-2})[38] and 3-1G(p) for H (α_{sp}=0.161 bohr^{-2} and α_d=1.10 bohr^{-2}).[36] The Hamiltonian matrix was diagonalized on 4 *k*-points (shrinking factor IS=2). We adopted default values for the tolerances controlling the accuracy of the Coulomb and exchange series. Atomic coordinates optimization was performed *via* an analytical gradient method, upgrading the numerical Hessian with the Broyden-Fletcher-Goldfarb-Shanno algorithm.[39] All graphical inspections were carried out with the molecular graphics program MOLDRAW,[40] and VMD[41] was employed for visualizing the electrostatic potential maps. The PBE vibrational frequencies were simulated at the *Γ* point within the harmonic approximation, by obtaining the eigenvalues from the diagonalization of the mass-weighted Hessian matrix.[42] The numerical gradient adopted a single displacement (0.003 Å) for each Cartesian coordinate of each atom with respect to the equilibrium configuration in order to build the Hessian matrix. The infrared intensity of each normal mode was calculated using the Berry phase approach.[43]

Molecular Dynamics Simulations

We used the ReaxFF version incorporated into the Amsterdam Density Functional (ADF) program for all the reactive molecular dynamics simulations.[44] These calculations were carried out in the gas phase, in the NVT ensemble using the Berendsen thermostat[45] with a relaxation constant of 0.1 ps. The equations of motion were solved with the velocity-Verlet algorithm[46] and the time step was set to 0.25 fs. During the equilibration phase, each system was energy minimized at T=10 K. Then, the temperature was gradually increased from 10K to 300K in 50 ps and the system was equilibrated at the final temperature for about 50 ps. After equilibration, the production simulations were carried out for 500 ps. Periodic boundary conditions were applied in all directions. Configurations were saved every 0.1 ps.

Results and discussion

The description of the plain surface model together with the acidic (-CH_2COOH) and basic (-CH_2NH_2) functionalization process is focused on structural, electronic and energetics features of the new models, computed at the PBE level, and on IR spectra, which are simulated for a direct comparison with the experimental results. In order to explore surface coverage and dynamics, the results of a series of classical reactive molecular dynamics simulations are reported and compared with the abovementioned static DFT calculations. The reactive force field used in this work was based on an earlier version but it has been re-parameterized by including all the models optimized at the QM level in the training set.

(101) α–cristobalite plain surface

Among the various candidates of crystalline silica apt to simulate a hydroxylated amorphous silica surface, the model of a (101) α–cristobalite surface, considered in a previous work,[30] was chosen for this study. In this model, the OH density (ρ = 4.8 OH/nm^2) is close to that of an amorphous silica outgassed at T < 400 K. At variance with the original model of Ref.[30], in this work, a supercell approach was adopted and the resulting geometry was fully optimized. The resulted reference cell of (101) cristobalite (hereafter named C101) with four–SiOH groups is shown in Figure 1 (top and side views, unit cell parameters: a = 8.61 Å, b = 10.05 Å, α=β=γ= 90°, surface area = 86.[49] Å^2).

Figure 1 shows silanol groups weakly interacting with each other via rather long H-bonds (2.00 Å). The electrostatic potential of the upper face of the C101 surface was mapped on the surface of the electron density enclosing 90% of the total electron density. The resulting map - reported in SI (Figure SI.1) – shows two markedly different areas: one with positive values of the potential due to the H of silanols (blue color in the Figure SI.1) and the other with negative values in correspondence with the oxygen of –SiOH groups (red colored regions in the map); the remaining part is neutral (green color). The comparison between the electrostatic potential of the functionalized models and the silanol reference

can be useful for shaping the modification of the electrostatic features of the original cristobalite surface occurred with the functionalization. These observations can shed light on the effects of the interactions between the substrate and the bonded biomolecules.

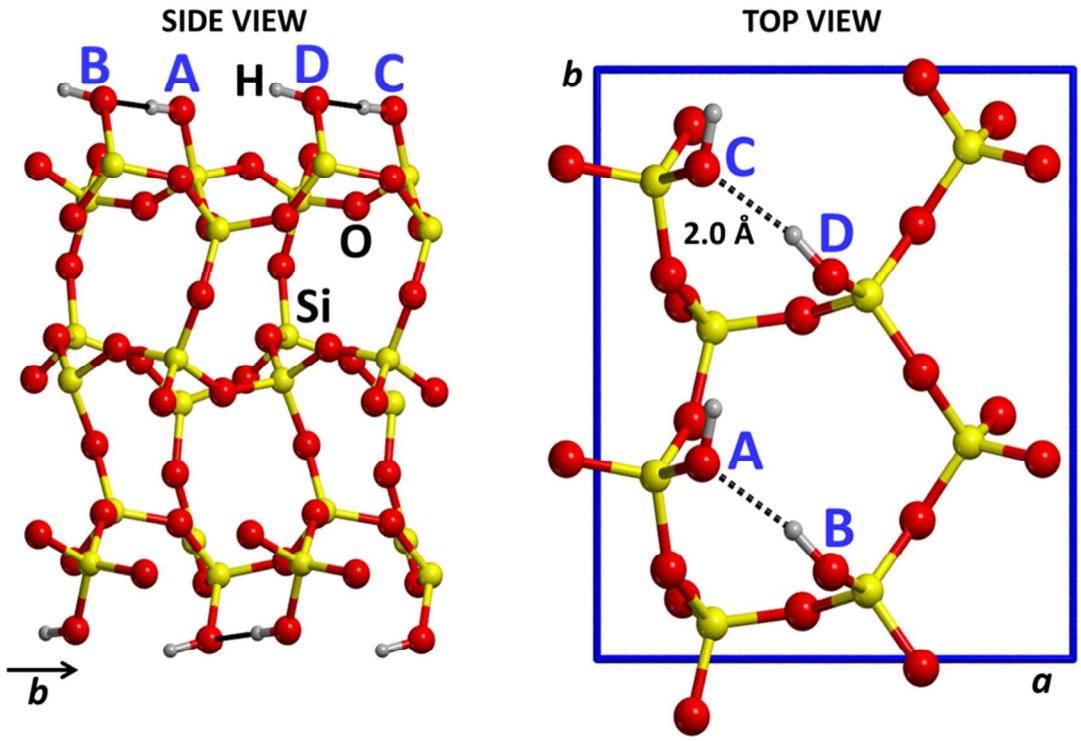

Figure 1. Model of the hydroxylated (101) cristobalite surface C101 with ρ(OH) = 4.8 OH/nm^2, viewed by side (left part) and on top (right part, only topmost atoms displayed for sake of clarity). Color coding: silicon yellow, oxygen red, hydrogen grey, H-bond black dotted line, unit cell borders blue. Silanol groups are labelled.

Acidic functionalization (-CH_2COOH)

The four available –SiOH groups exposed at the upper surface (*A, B, C* and *D* of Figure 1) were functionalized by substituting the -OH with the -CH_2COOH acidic termination. Formally, the process envisages the elimination of a water molecule and formation of a Si-C covalent bond, according to the following reference reaction

$$C101\text{-}n OH + n CH_3COOH \rightarrow C101\text{-}n CH_2COOH + n H_2O \qquad \text{(eq. 1)}$$

where *n* runs from 1 to 4 (labels A to D of Figure 1). This reaction does not reproduce a specific

experimental functionalization route, but represents an internal reference system to establish the relative stability of the considered models, as described in more details in this section.

The functionalized models were optimized by keeping the unit cell fixed to that of the plain C101 surface to mimic the rigidity of the bulk underneath. An increasing functionalization degree was considered by reaching n = 4, *i.e.* by the complete substitution of all silanol groups in the unit cell. Figure 2 reports the top view of all the optimized C101-$n$$CH_2COOH$ models, identified by the notation COOH-functionalized site(s).

For the case of n=2, three structures were designed and optimized, in order to take into account also the mutual interaction of the two –CH_2COOH functionalities. As displayed in Figure 2, for n = 2 we have modeled the following structures:1) *COOH-AB*, where the two acidic functionalities interact each one with the nearest remaining –SiOH via H-bond; 2) *COOH-BD-dim*, which corresponds to the quite strong direct mutual interaction among the two -CH_2COOH groups, with only the *A* silanol H-bonded to one of the two acidic terminations and 3) *COOH-BC-ring*, where the two acidic functionalities indirectly interact with each other due to the formation of a H-bond closed chain/ring, involving the two remaining -SiOH.

When 3 silanols were functionalized, two possible structures have been considered by comparing the results for n = 2. The difference is the presence/absence of the mutual interaction of two –CH_2COOH terminations, as in structure *COOH-ABD-dim* where the functionalized B and D are in mutual interaction and A is linked to the free C, with respect to *COOH-ABD* where B and D are not interacting (see Figure 2).

Finally, for the 100% coverage only the B and D –CH_2COOH groups are in mutual interaction while A and C are forced by steric hindrance to remain free from H-bonding interaction.

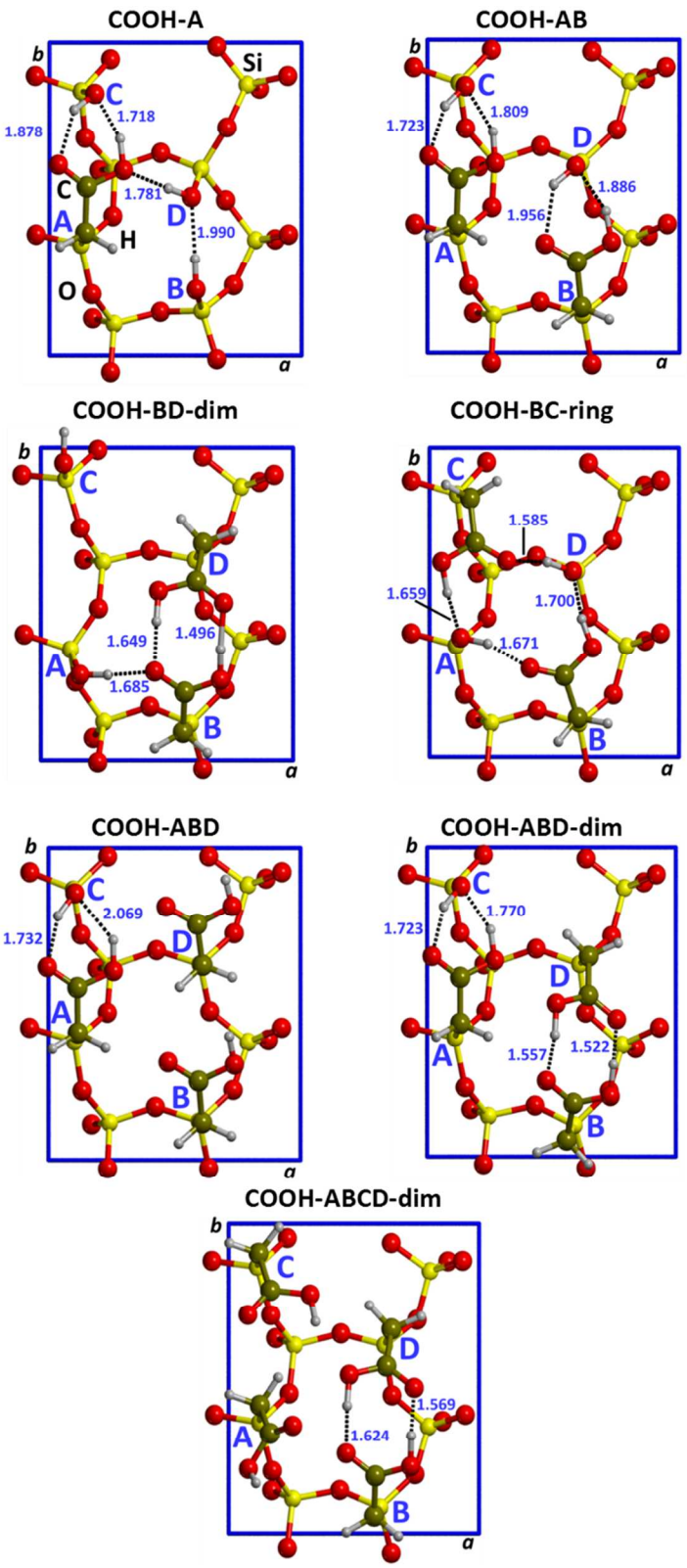

Figure 2. Top views of the optimized unit cell models at increasing degree of acidic -CH_2COOH functionalization of the cristobalite (101) surface. Numerical labels as H-bond lengths. Color coding: C: green, Si: yellow, O: red, H: grey, H-bond: black dotted line, unit cell borders: blue.

As highlighted in Figure 2, the most relevant geometrical features of the optimized models are the H-bond chains, which stabilize the resulting structure. For all but the *COOH-ABCD-dim* case, the –COOH group is always involved in two H-bonds either with a free silanol or with another –COOH. The average H-bond distance is 1.728 Å (± 0.150) and the strongest H-bonds are found in two structures with a -COOH groups in mutual interaction, *i.e.* the $O_{COD}\cdots H_{OHB}$ of 1.496 Å in *COOH-BD-dim* and 1.522 Å in *COOH-ABD-dim*.

Considering the electrostatic features of these models, the corresponding potential maps reported in the Supplementary Information reveal that the surface with just one acidic functionality has a poorly electro/nucleophilic character (blue/green in Figure SI.2). Only when the 100% coverage is reached the electrostatic potential becomes structured with clearly visible negative/positive regions (red areas in Figure SI.2). This is, however, due to the steric hindrance (*vide supra*) which forces the two acidic functionalities to move outside the natural position adopted when mutually interacting through H-bonds.

Table 1. Relative reaction energies for the reaction shown by equation 1, referred to the most stable case. Relative energies are in unit of kJ mol^{-1} and *per* functionalization degree (*n*). Labels refer to Figures 2 and 3, displaying the corresponding models.

ΔE	*A*	*AB*	*BC-ring*	*BD-dim*	*ABD*	*ABD-dim*	*ABCD*
n	1	2	2	2	3	3	4
-CH_2COOH	14.3	9.4	**0.0**	10.8	30.3	29.4	37.6
ΔE	*A*	*AC*			*ACD*		*ABCD*
-CH_2NH_2	**0.0**	5.2	-	-	48.2	-	58.0

To compare the relative stability of all the functionalized C101 structures of Figure 2, the energy differences per functionalization, corresponding to the reaction of eq. 1, were calculated and are

reported in Table 1, in order to rank the structures with respect the most stable one (shown by the value 0.0 in the Table). The most stable structure is *COOH-BC-ring*, *i.e.* the model where the two acidic terminations are part of a rather large closed chain of H-bonds involving two surface silanol groups. In this way, a ten-membered H-bonded ring is formed, which minimizes the steric constraints with respect to the two other cases, both higher in energy of 10.8 (*COOH-BD-dim*) and 9.4 kJ mol^{-1} (*COOH-AB*), respectively. The cases with three substitutions are all endoergonic with respect to the bi-substitution, as geometrical strain is not compensated for by the presence of H-bond interactions. This is also the case for the complete SiOH substitution, as steric hindrance does not allow the substituents A and C to interact through H-bond. It is then expected that at the experimental level only 50% of the available SiOH will be substituted by the acidic functionality.

Basic functionalization (-CH_2NH_2)

For the basic functionalization of the (101) cristobalite surface, four models were optimized and the resulting structures are reported in Figure 3. The H-bonds are less in number, as expected, and generally longer than the case of the acidic functionalization, although the average value of the H-bond distance is similar, 1.798 Å (± 0.175). Indeed, the shortest H-bond is 1.655 Å, for n = 1. With the increasing number of –CH_2NH_2 groups on the surface the H-bond distances become progressively longer as shorter SiOH$^{\cdots}NH_2$ H-bonds are substituted by longer HNH$^{\cdots}NH_2$ ones.

The electrostatic potential values mapped on the electronic density isosurface for the basic functionalization is reported in the Supplementary Information (Figure SI.3). In general, the maps show a dominant positive character, which increases moving from one to four –CH_2NH_2 group. The *NH_2-ABCD model* shows a highly electrophilic surface, due to the complete substitution of silanol groups with the CH_2NH_2 functionalities.

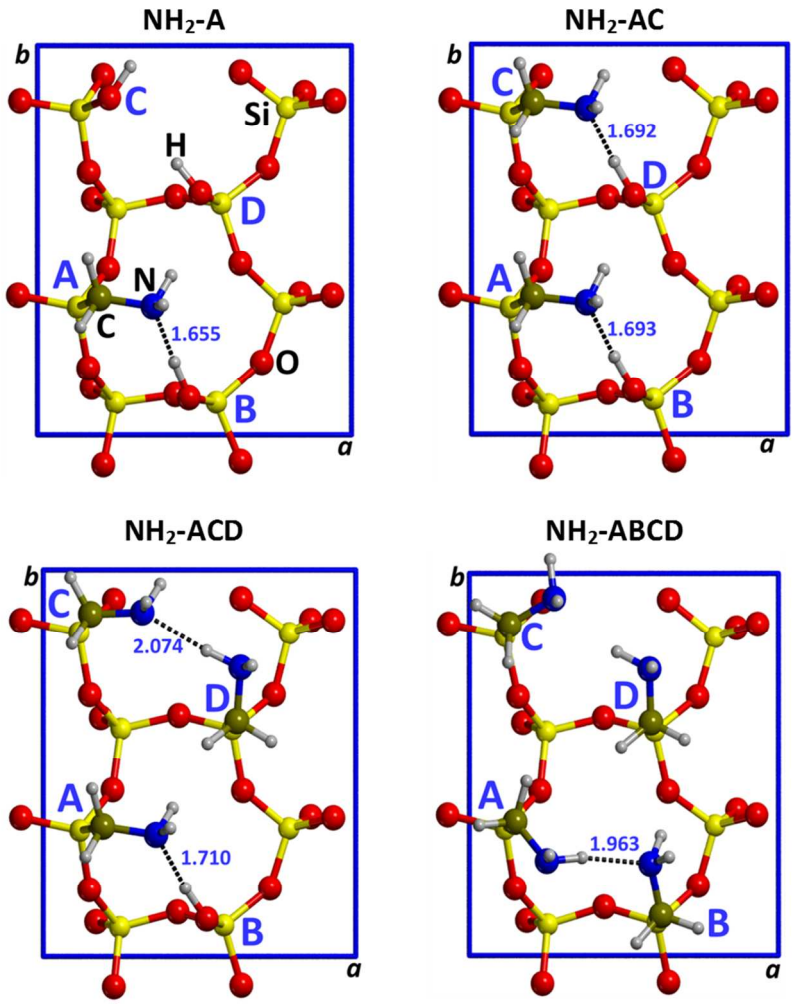

Figure 3. Top views of the optimized unit cell models at increasing degree of acidic -CH_2NH_2 functionalization on the cristobalite (101) surface. Numerical labels as H-bond lengths. Color coding: C: green, N: blue, Si: yellow, O: red, H: grey, H-bond: black dotted line, unit cell borders: blue.

Concerning the relative stability trend with respect to the increasing coverage, Table 1 shows that the most stable structure is that with one –CH_2NH_2 group. The energetic ranking follows the increase in functionalization number, with a significant jump in energy from n = 2 to n = 3 and 4, where H-bonds are longer or absent as for C and D functionalization in the *NH_2-ABCD* model.

IR spectra

The full IR spectra were simulated at Γ point within the harmonic approximation for all the described

models of Figures 2 and 3. In the following, we discuss, for sake of clarity, only a selection of the spectral regions involving the vibrational modes of COOH and NH_2 functionalities. Specifically, only the C=O stretching and NH_2 bending wavenumbers, which are good candidates for the experimental measurements, are described.

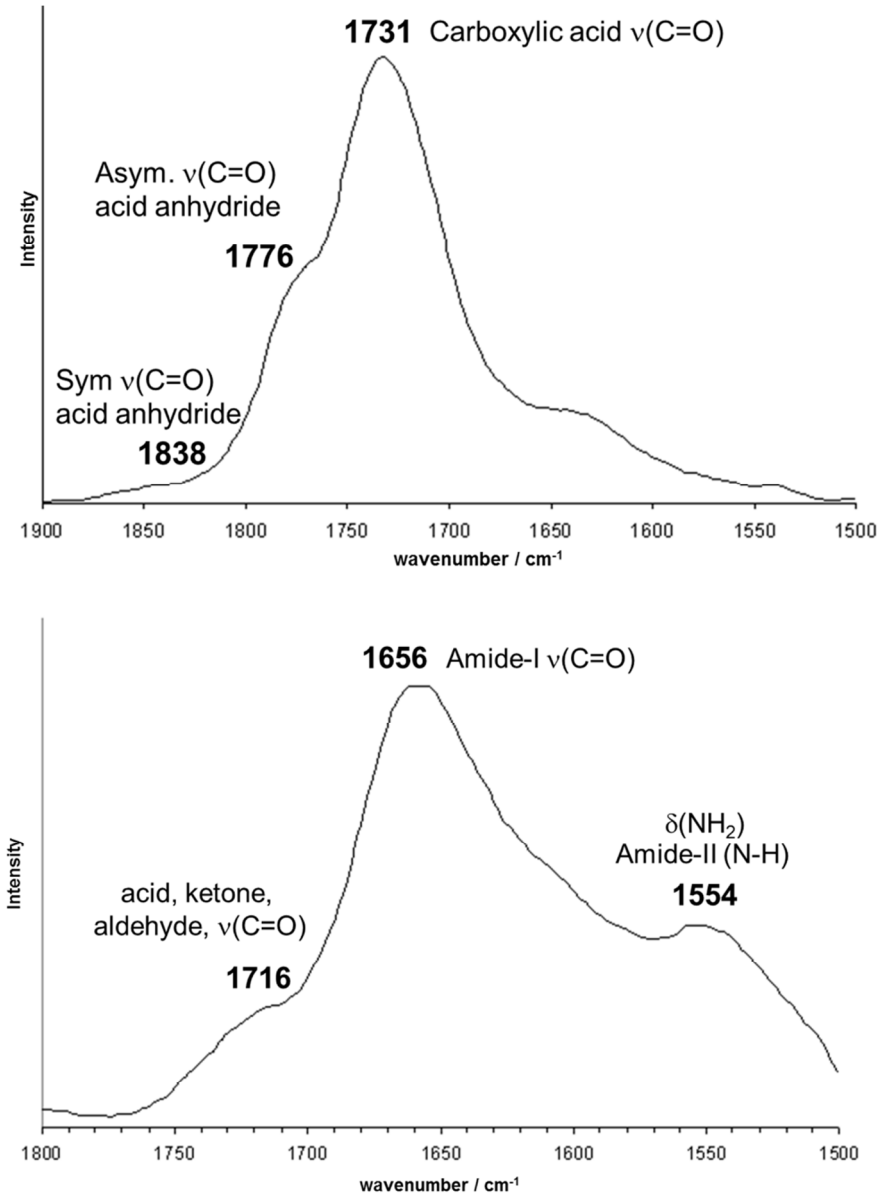

Figure 4. Experimental IR spectra of siloxane-based thin films carrying COOH (top spectrum) and NH_2 (bottom spectrum) chemical groups deposited by plasma processes. Assignments of the main features is also highlighted.

In Figure 4, the spectra in the 1500-1800 cm^{-1} region are shown for siloxane-based thin films carrying

COOH and NH_2 chemical groups deposited by using two different plasma processes based on pulsed electrical discharges. COOH-rich coatings have been achieved from the plasma co-polymerization of maleic anhydride and vinyltrimethoxylane,[23] whereas the plasma polymerization of 3-aminopropyl-triethoxasilane (APTES) gives rise to NH_2-rich layers.[47] Other data from a variety of experimental measurements on functionalized silica samples will also be discussed to compare with the computed data.

The case of CH_2COOH functionality. For the wavenumber of the C=O stretching mode of the CH_2COOH functionality (Figure 5), we refer to the value of a free CH_3COOH molecule (1851 cm^{-1}) for comparison. As C=O is usually involved in H-bond interaction, its wavenumber undergoes a bathochromic shift in comparison with the value of the free acetic acid. The minimum shift is -57 cm^{-1} (absolute vibration at 1794 cm^{-1} in Figure 5) corresponding to the coupled asymmetric C=O stretching of the CH_2COOH attached to silicon atoms *A* and *C* of the *COOH-ABCD-dim* model (see Figure 2). The very small shift is due to the non-interacting nature of the COOH groups attached at *A* and *C* sites. The maximum shift is -222 cm^{-1} (absolute value at 1629 cm^{-1} in Figure 5) for the CH_2COOH moiety named *B* in the *COOH-BD-dim* model engaged in two short H-bonds on the same oxygen atom of the C=O group (1.649 and 1.685 Å, see Figure 2). The most stable *COOH-BC-ring* model (see Table 1) shows two bands (1737 and 1707 cm^{-1}, for *C* and *B* substitution, respectively) shifted by -114 and -144 cm^{-1}, respectively. As the *COOH-BC-ring* model appears to be the most probable structure occurring on a hydroxylated silica surface with 4.8 OH/nm^2, this band pattern is the most informative one. However, the complexity of the resulting H-bond patterns, the dependency of the frequency values with the CH_2COOH surface loading and the static nature of the calculations do not allow to arrive to a clear cut picture of the ν(C=O) spectral features. When focusing on the bi-substituted cases (most probable from the energy point of view, see Table 1) configuration entropy will unfavorably bias *COOH-BD-*

dim over both *COOH-BC-ring* and *COOH-AB* models.

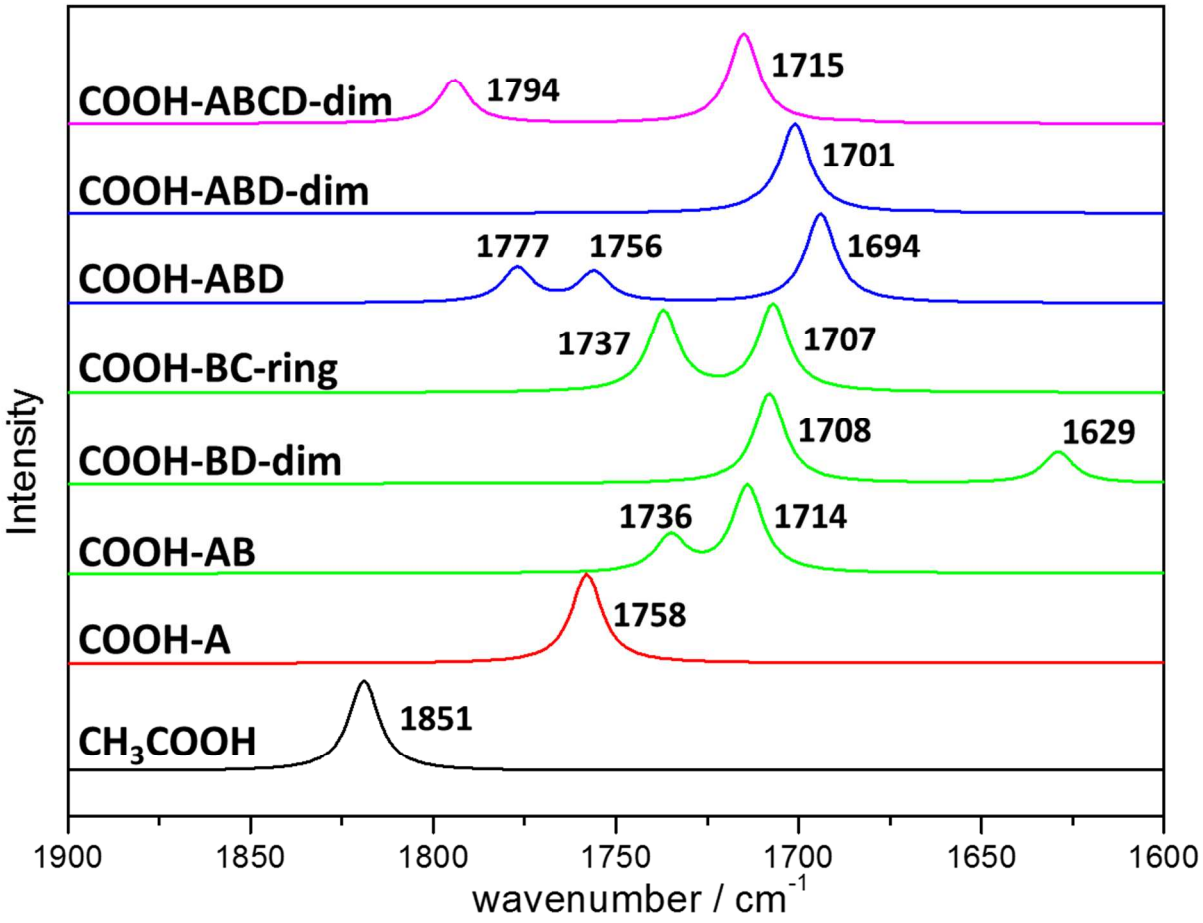

Figure 5. Computed IR spectra in the wavenumber region of the C=O stretching mode of the acidic cristobalite surface models displayed in Figure 2. Gas-phase acetic acid spectrum used as reference.

Considering that group mobility (not taken into account here) will significantly broad the ν(C=O) band, the simplest reference is the average of the four bands for the two considered models, resulting in a value of 1724 cm^{-1}. Within the above limitations, this value is not too far from the experimental FT-IR measurements around 1731 cm^{-1} reported in Figure 4 (top) on a COOH functionalized silica layer.[23] In a recent work[48] on the mesoporous silica (SBA-15) functionalized with butyric acid (CH_3-$(CH_2)_2$-COOH) a dependency of the C=O stretching frequency on the H-bond interactions with the surface silanol groups has been observed and discussed. Three cases were reported of the C=O stretching frequency value (1720, 1740 and 1750 cm^{-1}) as a function of the treatment temperature of the SBA-15

sample (373, 473 and 573 K). The authors interpreted the C=O stretching increasing value as due to two, one and zero H-bond donor surface SiOH groups to the C=O group. The increased outgassing temperature causes the condensation of the surface SiOH groups with a corresponding decreasing of the number of H-bond interactions with the C=O group. These data show that the sensitivity of the C=O frequency towards the H-bond environment is similar to what computed for the *COOH-AB* and *COOH-BC-ring* cases. A more tight comparison is not possible as the -CH_2COOH functional group used for the modeling is much closer to the silanol groups plane with respect to the experimental -CH_2-$(CH_2)_2$-COOH case, causing H-bond patterns with different features for the two systems.

The case of CH_2NH_2 functionality. Figure 6 shows the spectra for the CH_2NH_2 basic models centered in the NH_2 bending wavenumber region. In line with the acidic substitution case, the bending mode vibrating at 1632 cm^{-1} of the gas-phase CH_3NH_2 molecule has chosen as reference value. For all models but *NH_2-ACD* the $\delta(NH_2)$ value suffers a hypsochromic shift with respect to the value of the free CH_3NH_2 molecule at 1632 cm^{-1}. The only band suffering a bathochromic shift at 1609 cm^{-1} is for the *NH_2-ACD model* and is due to the group attached to silicon A (see Figure 3) in which the NH_2 group is acting exclusively as H-bond acceptor. As it is clear from Figure 6, the interpretation of the shift suffered by the $\delta(NH_2)$ mode is not straightforward. The IR spectra of aminopropyl-micelle template silicas reported in Ref.[49] show a rather complex and broadband in the 1590-1675 cm^{-1} region. Similarly, the spectral features of a siloxane-based thin films carrying NH_2 chemical groups as a result of a plasma polymerization of 3-aminopropyl-triethoxasilane (APTES) shown in Figure 4 (bottom) presents a broad feature around 1580 cm^{-1} to which the $\delta(NH_2)$ mode is contributing. One possible reason of the broadness of this band can be the sensitivity of the $\delta(NH_2)$ mode to the H-bonding interactions of the NH_2 groups with surface functionalities (both siloxane bonds and SiOH groups). To deepen the analysis, a series of calculations were run on simplified silica model of the *NH_2_A* model.

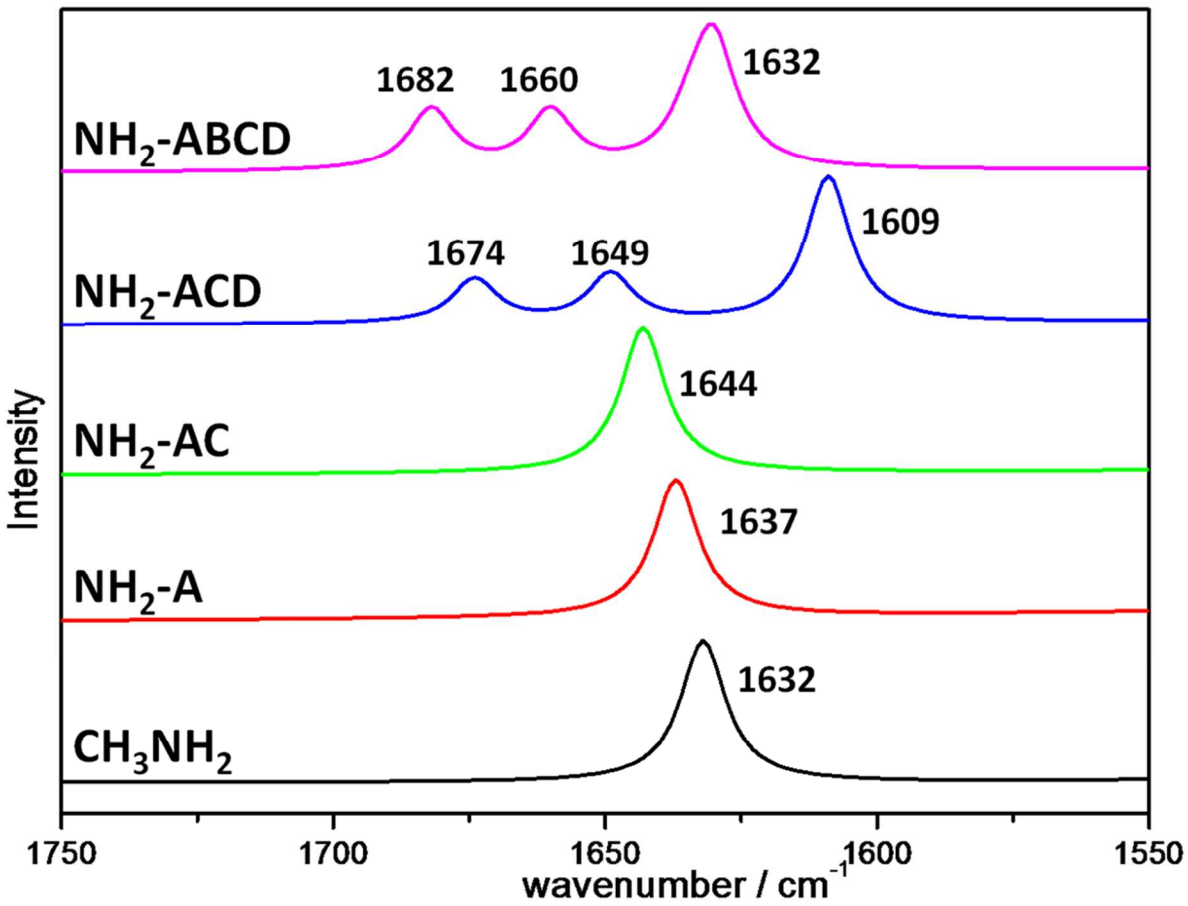

Figure 6. Computed IR spectra of the basic models displayed in Figure 4. The wavenumbers of the NH_2 bending region are reported for the increasing degree of functionalization.

To speed up the calculations, the silica slab thickness was reduced by keeping only the uppermost SiO_2 layer and saturating the underneath dangling bonds with hydrogen atoms. The model becomes, therefore, a single SiO_2 layer as shown in Figure 7. Despite the significant reduction in thickness, the comparison of the $\delta(NH_2)$ wavenumber values of the simplified model with that for the real slab gives a difference in wavenumber of only 2 cm^{-1} ($\delta(NH_2)$: 1635 cm^{-1} *vs* 1632 cm^{-1}), giving confidence for further calculations. To disentangle the origin of the $\delta(NH_2)$ shift, we have substituted the surface SiOH groups (involved in H-bonds) with Si-H groups (free from H-bonds). In this way, subsequent isolation of the NH_2 group from H-bonds with SiOH groups is attained. The last three cases shown in Figure 7 illustrate, respectively: i) NH_2 acting exclusively as a H-bond acceptor from a nearby silanol

group and the $\delta(NH_2)$ shifting to lower wavenumbers (1619 cm^{-1}); ii) NH_2 group acting exclusively as H-bond donor with respect to the nearby silanol group with the $\delta(NH_2)$ shifted to higher wavenumbers (1650 cm^{-1}); iii) a case similar to ii) but in which the NH_2 group is engaged in a much weaker H-bond with a siloxane bridge resulting in a value of the $\delta(NH_2)$ wavenumber only slightly shifted to higher values (1636 cm^{-1}) compared to the free value (1629 cm^{-1}).

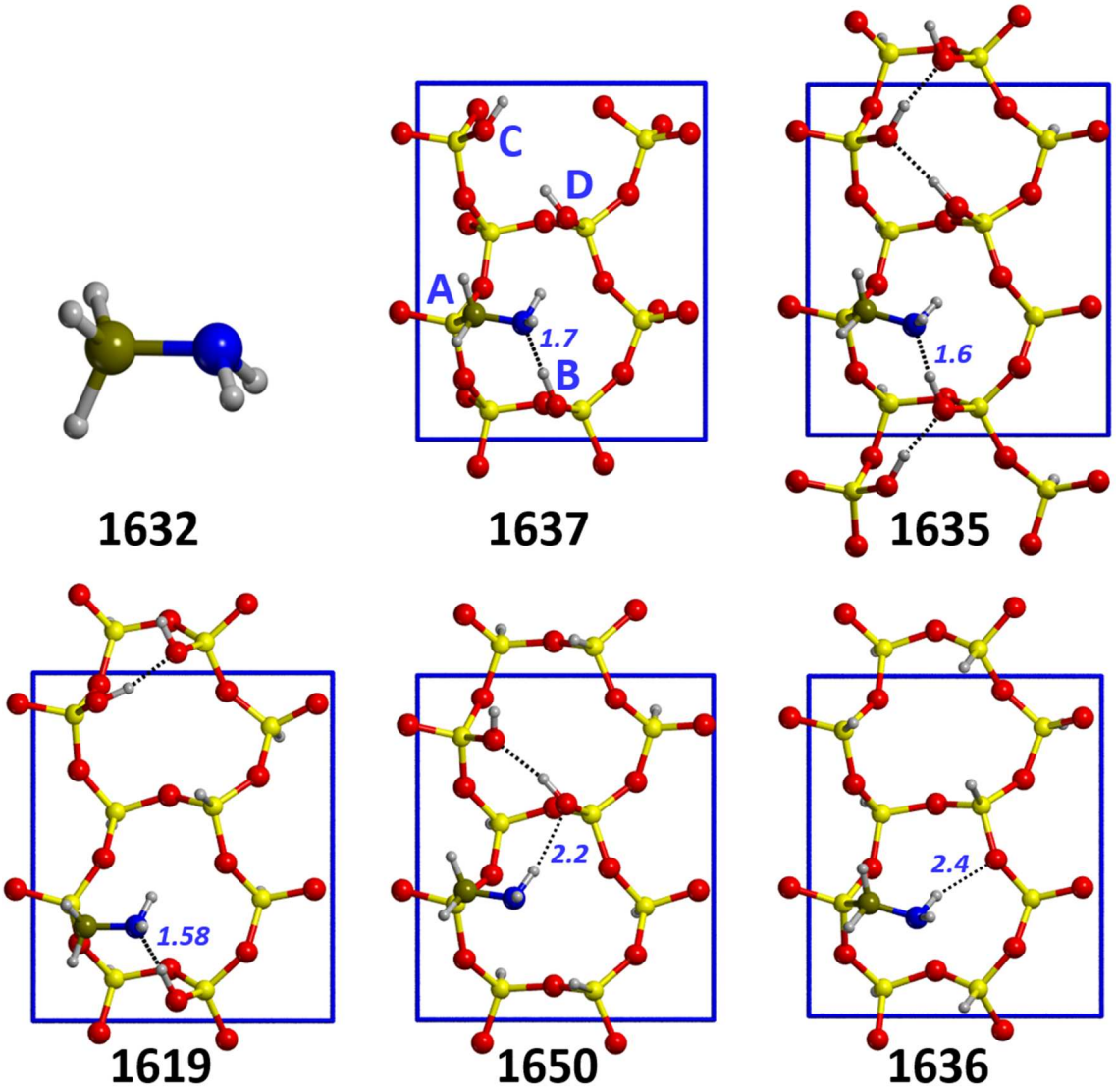

Figure 7. Simplified models of the original silica slab *NH_2-A model* in which OH groups are selectively substituted by H atoms. The $\delta(NH_2)$ bending frequency values (units of cm^{-1}) are shown and compared with the true slab case and with the CH_3NH_2 molecule. H-bonds shown as dotted lines. H-bond distances as blue labels in units of Å.

With this clear cut examples, the value of the wavenumber of the real slab (1637 cm^{-1}) can be interpreted as the average between hypsochromic and bathochromic shifts due to H-bonds involving NH_2 and D/B silanol groups, respectively. The lesson learned from the above analysis is that the $\delta(NH_2)$ frequency is an extremely sensitive probe of the local surrounding of the group and its interpretation in term of H-bond feature can be rather subtle. The broadness of the experimental band assigned to the $\delta(NH_2)$ mode can then be interpreted as a population of NH_2 groups involved in a web of H-bond interactions with the silica surface functionalities.

Molecular Dynamics Simulation

Mobility of the surface functionalities induced by thermal motion was studied by means of a classical reactive molecular dynamics approach, where the force field parameters were developed including in the training set some of the optimized quantum mechanical models studied in this work. Nevertheless, the paucity of both experimental and previous computational data on the system under study and the limitation of the force field only allow interpreting the results of the MD simulation in a qualitative fashion. In order to study the dynamical behavior of the substituted silica surfaces a more extended portion of the surface is needed to ensure a more realistic dynamic behavior. To that purpose, new models were defined by replicating the PBE-optimized unit cell three times in *x* and *y* directions. The final super-cell size was 25.821x30.144 $Å^2$ and the height of the simulation box was chosen large enough to prevent the mutual interaction of periodic images along *z*. The slab consisted of three layers of silicon atoms (216 in all) and 36 hydroxyl groups on each exposed face, available for functionalization. In order to generate various surface coverages, a number of surface hydroxyl groups was replaced by pre-optimized $-CH_2NH_2$ or $-CH_2COOH$ chains. Four starting configurations were prepared considering different percentages (25%, 50%, 75% and 100%) of substituted surface hydroxyl groups (Figures SI.4 and SI.5 in Supplementary Information). For each degree of functionalization, the

chains were located both far from each other and in a favorable interaction through intermolecular H-bonds, to compare different situations.

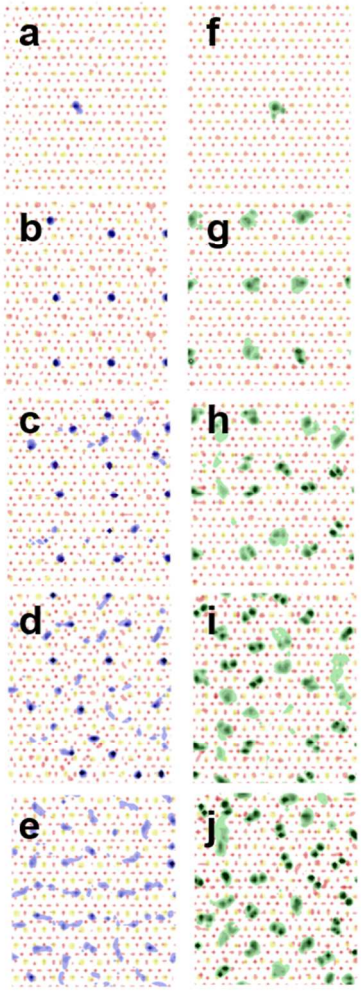

Figure 8. Two-dimensional probability density plots of the different percentages of $–CH_2NH_2$ (N: (blue): a=3%, b=25%, c=50%, d=75%, e=100%) and $–CH_2COOH$ (C: (green): f=3%, g=25%, h=50%, i=75%, j=100%) molecules in the *xy* plane of the (101) cristobalite surface (Si and O atoms are light yellow and red, respectively). Contour scales are in arbitrary units.

At low coverage (25%), the grafted chains are almost isolated and therefore do not interact with each other. Figure 8 shows the two-dimensional atomic density maps, revealing a very limited motion of the grafted chains. This is also confirmed by examining the atomic density profiles along the direction normal to the surface and the atomic radial distribution functions (see Figures reported in the SI). This is especially evident in the case of amine chains where the areas explored by the chain head groups,

represented by blue spots in the 2D density contours (Figure 8), are essentially confined to the center of the "dodecagon" rings of the interface. Indeed, after a brief (a few picoseconds) exploration of the surroundings, the chains orient the amine hydrogen atoms towards the surface and become engaged in intermolecular H-bonds with the remaining SiOH groups of the silica layer. These active portions, in turn, re-align, concertedly, the oxygen lone pairs with the NH bonds and maximize their interactions with the chains: two H-bonds act as linkers and keep the CH_2NH_2 moieties close to the surface at an average distance of about 1.75 Å (see Figure SI.6b). Nitrogen atoms are located far from each other at distances of about 8.5 or 10 Å, whereas they are prevalently close to the oxygen atoms of the surface at a distance of about 3.3 Å (see N-O and N-N radial distribution functions of Figure SI.7). However, this distance is slightly longer than the one estimated in the single molecule case (2.98 Å).

Inspection of the atomic density maps for the CH_2COOH chain for lower coverage (25%), shows a rather large mobility as wider areas of the surface are explored during the chain motion (Figure 8); the oxygen atoms remain farther from the top layer of the slab (Figure SI.6) and only one H-bond per molecule is engaged with the interface, on average.

On the contrary, at higher concentrations (50-100%) both substituents (-CH_2NH_2 and –CH_2COOH) are mobile and self-interact through a dense and dynamic network of intermolecular H-bonds. No privileged orientations are observed as shown by the broader contour plots and distributions shown in Figures 8, SI.6 and SI.9. Nitrogen atoms can be found very close to each other (3.7 Å) and are located farther from the surface (at an average z-distance of about 2.1 Å – Figure SI.6). They are coordinated by a lower number of surface oxygen atoms (5 on average, as estimated from the integration of the radial distribution functions of Figure SI.7) in relation to the low concentration case, where they are 7, on average. Carboxyl groups are preferentially found far from the layer due to the unfavorable interactions with the oxygen atoms of the surface.

At variance with the CH_2NH_2 case, the distinction between low and high concentration is not so

evident in the -CH_2COOH functionalization. The shifts of the high concentration RDF peaks to shorter distances (Figure SI.8) only suggest the presence of inter-headgroup H-bonds, which could not be observed when the molecule are grafted far from each other.

Moreover, in line with other theoretical investigations,[50-52] the relative stability of different coverage percentages was evaluated by comparing the average packing energy per chain (either CH_2NH_2 or CH_2COOH). This quantity was estimated from the production runs in the gas phase at T=300 K and was calculated as:

$$\Delta E_{pack} = \frac{\bar{E}_{Surf+SAM} - \bar{E}_{Surf} - n\bar{E}_{Chain}}{n} \quad (2)$$

where $\bar{E}_{Surf+SAM}$ is the average energy of the functionalized system, $\bar{E}_{Surf}$ is the average energy of the surface without functionalizing chains and $\bar{E}_{Chain}$ is the average energy *per* chain (n is the number of substituted sites or grafted chains). Packing energies differences are reported in Table 2.

Table 2. Intermolecular H-bonds between chain head groups and surface silanol groups expressed through atom-atom radial distribution functions RDF (see Figures SI.7 and SI.8). Only the peak identifying the selected type of hydrogen bond is reported (distance between the involved atoms in Å) and area under the peak (coordination number). RDF [O(COOH)…H(OH)] identifies the peak position between the sp^2 oxygen atom of the COOH group and the hydrogen atom of the silanol group. Other labels follow the same convention. Relative packing energies (equation 2), referred to the most stable case. Relative energies are in unit of kJ·mol^{-1}. For 100% coverage, ΔE_{pack} is 126 and 134 kJ·mol^{-1}, for $-CH_2COOH$ and $-CH_2NH_2$, respectively.

-CH_2COOH	ΔE_{pack}	RDF [O(COOH) ⋯ H(OH)]		RDF [H(COOH) ⋯ O(OH)]	
Coverage %		Peak position	Coord. #	Peak position	Coord. #
25	13	2.25	1.2	1.85	1.3
50	29	1.65	0.8	1.85	1.3
75	**0**	**1.65**	**1.1**	**1.85**	**1.1**
-CH_2NH_2	ΔE_{pack}	RDF [N(NH_2) ⋯ H(OH)]		RDF [H(NH_2) ⋯ O(OH)]	
Coverage %		Peak position	Coord. #	Peak position	Coord. #
25	**0**	**2.16**	**4.4**	**1.54**	**0.6**
50	75	2.16	4.0	1.96	1.1
75	213	3.40	2.8	1.95	1.2

As far as amine grafting is concerned, the most stable functionalization appears to be the one obtained

at low coverage (25%) whereas in the case of carboxyl attachment the most favorable arrangement is achieved with a 75% substitution. This is in line with the positions and coordination numbers of the first peaks of the radial distribution functions identifying the most important H-bonds between the surface and the chains (Table 2).

Indeed, the best coverages correspond to structures characterized by stronger contacts (with shorter distances between the atoms forming the hydrogen bonds) between the chains head groups and the silanol groups of the surface. At higher NH_2 concentrations, the average grafting energy is less favorable presumably because of less favorable intermolecular interactions between the chain head groups and the surface, which should be stronger than the interactions between the head groups themselves.

Conclusions

Acidic (CH_2COOH) and basic (CH_2NH_2) functionalization of the (101) cristobalite surface, assumed as a model of hydroxylated amorphous silica surface, have been simulated and characterized in terms of their electrostatic and vibrational properties to design a functionalized material apt to attach biomolecules by chemical condensation with the exposed functionalities. The increasing loading of functionalities from 1 to 4 per surface unit cell has been studied, to investigate the number and strength of the interactions with either the remaining surface silanol groups or between functionalities. For the –CH_2NH_2 chain, functionalized surfaces become less stable with increasing loading of the functionalizing groups. On the contrary, the functionalization with the –CH_2COOH chain is more stable at higher loading, probably due to an increased number of favorable H-bonding contacts.

The simulation of the IR spectra offered a tool to interpret experimental spectra in the C=O stretching and NH_2 bending regions, for the –CH_2COOH and –CH_2NH_2 functionalities, respectively. It is shown that, for the –CH_2COOH functionality, the most prominent spectral feature is around 1727 cm^{-1} as an

average, in reasonable agreement with experiment once considering the approximations of the modeling approach. For the NH_2 bending mode, a more involved behavior of the corresponding band is predicted. As a function of the involvement of the NH_2 moiety as either H-bonding donor (weak) or acceptor (strong), the resulting bending frequency value moves up or down with respect to a completely free NH_2 reference group. However, the resulting shift in the NH_2 bending frequency cannot be easily foreseen from the local geometrical surrounding of the CH_2NH_2 chain due to a different sensitivity of the frequency when behaving as either H-bond donor or acceptor. This is an important fact to be considered for interpreting experimental spectra in the NH_2 region, as small shifts with respect to a "free from interaction" value may result from the cancellation of opposite effects on the NH_2 bending frequency.

The molecular dynamics calculations based on ReaxFF force field performed over larger unit cell revealed a complex chains motion with some higher mobility of the CH_2COOH chain with respect to the CH_2NH_2 one. Despite the complexity of the system and the differences between DFT and ReaxFF approaches, both predicted a preference for low coverage when CH_2NH_2 chain is involved at variance with higher coverage values for the CH_2COOH chain. This has been attributed to the number and strength of H-bonds at the functionalized surfaces.

The results of this work are a fundamental step in the surface characterization process and suggest that the developed methodology can be confidently applied to the simulation of extended realistic models of amorphous silica surfaces. Indeed, work is already in progress in our laboratory envisaging the adoption of more realistic models for the amorphous silica surface, which will also become the candidate to study the attachment of amino acids and oligopeptides to the surface.

Acknowledgements

This research was carried out in the framework of the European M-ERA.NET BioADBD project

funded by the Luxembourgish agency "Fonds National de la Recherche" (FNR-INER/MAT/11/01). Marta Corno and Piero Ugliengo acknowledge Progetti di Ricerca di Ateneo–Compagnia di San Paolo-2011-Linea 1A, progetto ORTO11RRT5 for funding. Susanna Monti is grateful to Adri C. T. van Duin for the serial version of the reactive dynamics program (ReaxFF), for his useful comments and suggestions. Fruitful discussion with Barbara Onida (Politecnico of Torino) is also acknowledged.

Associated Content

Supporting Information Available: electrostatic potential mapped on the electron density isosurface for all the surface models described – plain cristobalite (101) surface, -CH_2COOH and –CH_2NH_2 functionalized structures (Figures SI.1 to SI.3); models used for Molecular Dynamics calculations for both basic (Figure SI.4) and acid (Figure SI.5) functionalization from 3 to 100% coverage; normalized Z-density distributions of the distances of carboxylic oxygen and nitrogen form surface silicon (Figure SI.6); atom-atom radial distribution functions (RDFs) for both acidic (Figure SI.7) and basic (Figure SI.8) cases; normalized distributions of the number of contacts between nitrogen or oxygen of functionalities and all the oxygen atoms in the simulation cell (Figure SI.9).

References

1. Wilson, C. J.; Clegg, R. E.; Leavesley, D. I.; Pearcy, M. J. Mediation of Biomaterial-Cell Interactions by Adsorbed Proteins: A Review. *Tissue Eng.* **2005,** *11* (1-2), 1-18.
2. Kasemo, B.; Gold, J. Implant Surfaces and Interface Processes. *Adv. Dent. Res.* **1999,** *13*, 8-20.
3. Hoffmann, F.; Cornelius, M.; Morell, J.; Fröba, M. Silica-Based Mesoporous Organic-Inorganic Hybrid Materials. *Angew. Chem., Int. Ed.* **2006,** *45* (20), 3216-3251.
4. Meder, F.; Kaur, S.; Treccani, L.; Rezwan, K. Controlling Mixed-Protein Adsorption Layers on Colloidal Alumina Particles by Tailoring Carboxyl and Hydroxyl Surface Group Densities. *Langmuir* **2013,** *29* (40), 12502-12510.
5. Iler, R. K. *The Chemistry of Silica: Solubility, Polymerization, Colloid and Surface Properties and Biochemistry*. Wiley-Interscience: New York, 1979.
6. Liong, M.; Lu, J.; Kovochich, M.; Xia, T.; Ruehm, S. G.; Nel, A. E.; Tamanoi, F.; Zink, J. I. Multifunctional Inorganic Nanoparticles for Imaging, Targeting, and Drug Delivery. *ACS Nano* **2008,** *2* (5), 889-896.

7. Kresge, C. T.; Leonowicz, M. E.; Roth, W. J.; Vartuli, J. C.; Beck, J. S. Ordered Mesoporous Molecular Sieves Synthesized by a Liquid-Crystal Template Mechanism. *Nature* **1992,** *359* (6397), 710-712.
8. Rosenholm, J. M.; Lindén, M. Towards Establishing Structure–Activity Relationships for Mesoporous Silica in Drug Delivery Applications. *J. Control. Release* **2008,** *128* (2), 157-164.
9. Vallet-Regi, M.; Balas, F.; Arcos, D. Mesoporous Materials for Drug Delivery. *Angew. Chem., Int. Ed.* **2007,** *46* (40), 7548-7558.
10. Zhuravlev, L. T. Concentration of Hydroxyl-Groups on the Surface of Amorphous Silica. *Langmuir* **1987,** *3* (3), 316-318.
11. Zhuravlev, L. T. The Surface Chemistry of Amorphous Silica. Zhuravlev Model. *Colloid Surf. A-Physicochem. Eng. Asp.* **2000,** *173* (1-3), 1-38.
12. Puddu, V.; Perry, C. C. Interactions at the Silica-Peptide Interface: The Influence of Particle Size and Surface Functionality. *Langmuir* **2014,** *30* (1), 227-233.
13. Pujari, S. P.; Scheres, L.; Marcelis, A. T. M.; Zuilhof, H. Covalent Surface Modification of Oxide Surfaces. *Angew. Chem., Int. Ed.* **2014,** *53*, 2-36.
14. Builes, S.; Vega, L. F. Understanding CO2 Capture in Amine-Functionalized MCM-41 by Molecular Simulation. *J. Phys. Chem. C* **2012,** *116* (4), 3017-3024.
15. Datt, A.; El-Maazawi, I.; Larsen, S. C. Aspirin Loading and Release from MCM-41 Functionalized with Aminopropyl Groups Via Co-Condensation or Postsynthesis Modification Methods. *J. Phys. Chem. C* **2012,** *116* (34), 18358-18366.
16. Calvo, A.; Angelome, P. C.; Sanehez, V. M.; Scherlis, D. A.; Williams, F. J.; Soler-Illia, G. Mesoporous Aminopropyl-Functionalized Hybrid Thin Films with Modulable Surface and Environment-Responsive Behavior. *Chem. Mat.* **2008,** *20* (14), 4661-4668.
17. Gessner, A.; Lieske, A.; Paulke, B. R.; Müller, R. H. Functional Groups on Polystyrene Model Nanoparticles: Influence on Protein Adsorption. *J. Biomed. Mater. Res. A* **2003,** *65A* (3), 319-326.
18. Csőgör, Z.; Nacken, M.; Sameti, M.; Lehr, C. M.; Schmidt, H. Modified Silica Particles for Gene Delivery. *Mat. Sci. Eng.: C* **2003,** *23* (1-2), 93-97.
19. Slowing, I.; Brian, G. T.; Victor, S. Y. L. Effect of Surface Functionalization of MCM-41-Type Mesoporous Silica Nanoparticles on the Endocytosis by Human Cancer Cells. *J. Am. Chem. Soc.* **2006,** *128*, 14792-14793.
20. Doadrio, J. C.; Sousa, E. M. B.; Izquierdo-Barba, I.; Doadrio, A. L.; Perez-Pariente, J.; Vallet-Regí, M. Functionalization of Mesoporous Materials with Long Alkyl Chains as a Strategy for Controlling Drug Delivery Pattern. *J. Mat. Chem.* **2006,** *16* (5), 462-466.
21. Soto-Cantu, E.; Cueto, R.; Koch, J.; Russo, P. S. Synthesis and Rapid Characterization of Amine-Functionalized Silica. *Langmuir* **2012,** *28* (13), 5562-5569.
22. Tsai, H.-H. G.; Jheng, G.-L.; Kao, H.-M. Direct Evidence for Interactions between Acidic Functional Groups and Silanols in Cubic Mesoporous Organosilicas. *J. Am. Chem. Soc.* **2008,** *130* (35), 11566-11567.
23. Mauchauffe, R.; Moreno-Couranjou, M.; Boscher, N. D.; Weerdt, C. V. D.; Duwez, A.-S.; Choquet, P. Robust Bio-Inspired Antibacterial Surfaces Based on the Covalent Binding of Peptides on Functional Atmospheric Plasma Thin Films. *J. Mater. Chem. B* **2014**.
24. Rimola, A.; Costa, D.; Sodupe, M.; Lambert, J.-F.; Ugliengo, P. Silica Surface Features and Their Role in the Adsorption of Biomolecules: Computational Modeling and Experiments. *Chem. Rev.* **2013,** *113*, 4216-4313.
25. Builes, S.; Lopez-Aranguren, P.; Fraile, J.; Vega, L. F.; Domingo, C. Alkylsilane-Functionalized Microporous and Mesoporous Materials: Molecular Simulation and Experimental Analysis of Gas Adsorption. *J. Phys. Chem. C* **2012,** *116* (18), 10150-10161.

26. Builes, S.; Vega, L. F. Effect of Immobilized Amines on the Sorption Properties of Solid Materials: Impregnation Versus Grafting. *Langmuir* **2013,** *29* (1), 199-206.
27. Williams, J. J.; Seaton, N. A.; Dueren, T. Influence of Surface Groups on the Diffusion of Gases in MCM-41: A Molecular Dynamics Study. *J. Phys. Chem. C* **2011,** *115* (21), 10651-10660.
28. Zhu, Y.; Zhou, J.; Hu, J.; Liu, H. The Effect of Grafted Amine Group on the Adsorption of CO2 in MCM-41: A Molecular Simulation. *Catal. Today* **2012,** *194* (1), 53-59.
29. Dkhissi, A.; Esteve, A.; Jeloaica, L.; Esteve, D.; Rouhani, M. D. Self-Assembled Monolayers and Preorganization of Organosilanes Prior to Surface Grafting onto Silica: A Quantum Mechanical Study. *J. Am. Chem. Soc.* **2005,** *127* (27), 9776-9780.
30. Musso, F.; Sodupe, M.; Corno, M.; Ugliengo, P. H-Bond Features of Fully Hydroxylated Surfaces of Crystalline Silica Polymorphs: A Periodic B3LYP Study. *J. Phys. Chem. C* **2009,** *113* (41), 17876-17884.
31. Perdew, J. P.; Burke, K.; Enzerhof, M. Generalized Gradient Approximation for the Exchange-Correlation Hole of a Many-Electron System. *Phys. Rev. Lett.* **1996,** *77*, 3865.
32. Dovesi, R.; Civalleri, B.; Orlando, R.; Roetti, C.; Saunders, V. R. Ab Initio Quantum Simulation in Solid State Chemistry. *Rev. Comp. Chem.* **2005,** *21*, 1-125.
33. Dovesi, R.; Orlando, R.; Civalleri, B.; Roetti, C.; Saunders, V. R.; Zicovich-Wilson, C. M. CRYSTAL: A Computational Tool for the Ab Initio Study of the Electronic Properties of Crystals. *Z. Kristall.* **2005,** *220*, 571-573.
34. Dovesi, R.; Saunders, V. R.; Roetti, C.; Orlando, R.; Zicovich-Wilson, C. M.; Pascale, F.; Civalleri, B.; Doll, K.; Harrison, N. M.; Bush, I. J., et al. *CRYSTAL09, User's Manual*. 2009.
35. Civalleri, B.; Zicovich-Wilson, C. M.; Ugliengo, P.; Saunders, V. R.; Dovesi, R. A Periodic Ab Initio Study of the Structure and Relative Stability of Silica Polymorphs. *Chem. Phys. Lett.* **1998,** *292*, 394.
36. Corno, M.; Busco, C.; Civalleri, B.; Ugliengo, P. Periodic Ab Initio Study of Structural and Vibrational Features of Hexagonal Hydroxyapatite Ca10(PO4)6(OH)2. *Phys. Chem. Chem. Phys.* **2006,** *8*, 2464-2472.
37. Catti, M.; Pavese, A.; Dovesi, R.; Saunders, V. C. Static Lattice and Electron Properties of MgCO3 (Magnesite) Calculated by Abinitio Periodic Hartree-Fock Methods. *Phys. Rev. B* **1993,** *47*, 9189-9198.
38. Gatti, C.; Saunders, V. R.; Roetti , C. Crystal-Field Effects on the Topological Properties of the Electron-Density in Molecular-Crystals - the Case of Urea. *J. Chem. Phys.* **1994,** *101*, 10686-10696.
39. Dovesi, R.; Saunders, V. R.; Roetti, C.; Orlando, R.; Zicovich-Wilson, C. M.; Pascale, F.; Civalleri, B.; Doll, K.; Harrison, N. M.; Bush, I. J., et al. University of Turin: CRYSTAL2009 User's Manual. Turin, 2009.
40. Ugliengo, P.; Viterbo, D.; Chiari, G. MOLDRAW: Molecular Graphics on a Personal Computer. *Z. Kristall.* **1993,** *208* (Part-2), 383-383.
41. Humphrey, W.; Dalke, A.; Schulten, K. VMD: Visual Molecular Dynamics. *J. Mol. Graph.* **1996,** *14* (1), 33-8, 27-8.
42. Pascale, F.; Zicovich-Wilson, C. M.; Gejo, F. L.; Civalleri, B.; Orlando, R.; Dovesi, R. The Calculation of the Vibrational Frequencies of Crystalline Compounds and Its Implementation in the CRYSTAL Code. *J. Comput. Chem.* **2004,** *25* (6), 888-897.
43. Noel, Y.; Zicovich-Wilson, C. M.; Civalleri, B.; D'Arco, P.; Dovesi, R. Polarization Properties of ZnO and BeO: An Ab Initio Study through the Berry Phase and Wannier Functions Approaches. *Phys. Rev. B.* **2001,** *65*, 014111-014120.
44. Baerends, E. J.; Ziegler, T.; Autschbach, J.; Bashford, D.; Bérces, A.; Bickelhaupt, F. M.; Bo, C.; Boerrigter, P. M.; Cavallo, L.; Chong, D. P., et al. *ADF2012.01a Scm Theoretical Chemistry*. Vrije Universiteit: Amsterdam, The Netherlands, 2012.

45. Berendsen, H. J. C.; Postma, J. P. M.; van Gunsteren, W. F.; DiNola, A.; Haak , J. R. Molecular-Dynamics with Coupling to an External Bath. *J. Chem. Phys.* **1984,** *81*, 3684–3690.
46. Allen, M. P.; Tildesley , D. J. *Computer Simulations of Liquids*. Clarendon Press: Oxford, 1989.
47. Lecoq, E.; Bulou, S.; Gueye, M.; Gries, T.; Noel, C.; Belmonte, T.; Choquet, P. NH2-Siloxane Layers Deposited in an Ar-N2 Microwave Afterglow Using 3-Aminopropyltriethoxysilane (APTES): How to Improve the Amino-Group Retention? In *14th International Conference on Plasma Surface Engineering*, Garmisch-Partenkirchen (Germany), 2014.
48. Fiorilli, S.; Camarota, B.; Garrone, E.; Onida, B. Carboxylic Groups in Mesoporous Silica and Ethane-Bridged Organosilica: Effect of the Surface on the Reactivity. *Phys. Chem. Chem. Phys.* **2011,** *13* (3), 1201-1209.
49. Brunel, D.; Blanc, A. C.; Garrone, E.; Onida, B.; Rocchia, M.; Nagy, J. B.; Macquarrie, D. J. Spectroscopic Studies on Aminopropyl-Containing Micelle Templated Silicas. Comparison of Grafted and Co-Condensation Routes. In *Studies in Surface Science and Catalysis*, R. Aiello, G. G.; Testa, F., Eds. Elsevier: 2002; Vol. 142, pp 1395-1402.
50. Jang, Y. H.; Jang, S. S.; Goddard, W. A. Molecular Dynamics Simulation Study on a Monolayer of Half [2]Rotaxane Self-Assembled on Au(111). *J. Am. Chem. Soc.* **2005,** *127*, 4959-4964.
51. Pei, Y.; Ma, J.; Jiang, Y. Formation Mechanisms and Packing Structures of Alkoxyl and Alkyl Monolayers on Si(111): Theoretical Studies with Quantum Chemistry and Molecular Simulation Models. *Langmuir* **2003,** *19*, 7652-7661.
52. Zhang, L.; Wesley, K.; Jiang, S. Molecular Simulation Study of Alkyl Monolayers on Si(111). *Langmuir* **2001,** *17*, 6275-6281.

Toc Graphics